A Model for Short Residence Time Hydropyrolysis of Single Coal Particles

WILLIAM B. RUSSEL
and
DUDLEY A. SAVILLE
Department of Chemical Engineering
Princeton University
Princeton, New Jersey 08540
and
MARVIN I. GREENE
Cities Service Research and
Development Company
Cranbury, New Jersey 08512

The chemical reactions and mass transfer processes occurring within a single coal particle during high temperature hydropyrolysis are described mathematically and the model is tested using extant experimental data. A significant feature of the model is the treatment of bulk flow due to the evolution of volatiles and the resulting balance between diffusion, bulk flow, and chemical reaction. Predictions of the variations in conversion due to changes in total pressure, hydrogen partial pressure, and particle size agree quantitatively with experimental data.

SCOPE

The objectives of this study were to develop a model of the chemical reactions and transport processes taking place within a small coal particle after exposure to hot hydrogen at high pressures and to test the predictions using extant experimental data. Such a model provides a means for understanding the effects of process variables (principally temperature, pressure, particle size, and residence time) on the yields from a given coal. Previous work on single-particle models focuses on the various chemical reaction rates and either ignores mass transport processes completely or lumps the resistance into a film coefficient. Although such models can often be adjusted to fit data for a given particle size, the sharp increase in yield observed as particle size is decreased appears to be beyond their predictive capabilities. To illustrate the role of mass transfer by bulk flow and diffusion, the kinetics of the devolatilization process and the time temperature history of the particle have been simplified by assuming a single first-order devolatilization reaction, instantaneous heatup to an isothermal state, and a long reaction time.

CONCLUSIONS AND SIGNIFICANCE

A theory has been developed to describe the chemical reactions and mass transfer processes occurring in a single coal particle during hydropyrolysis. The particle is assumed to maintain a porous structure throughout decomposition, with volatiles transported by diffusion and hydrodynamic flow. Chemical reactions are described in terms of the weight loss kinetics developed by previous workers and include the primary devolatilization of the coal, secondary reactions of free radicals, and direct hydrogenation of char. Order of magnitude estimates are used to show that bulk flow and the combination of free radicals with hydrogen are rapid compared to devolatilization, while diffusion is generally slow. The corresponding mathematical simplifications in the conservation equations lead to analytical solutions for the instantaneous rate of evolution of volatiles. Total yields obtained by integrating over an idealized temperature history agree closely with experimental data for variations in pressure, hydrogen partial pressure, and particle size. Close agreement with experimental data is obtained for the effect of temperature on pyrolysis at low and high pressure in inert atmospheres, but for hydropyrolysis at 69 atm it is poor owing, evidently, to the simplified kinetic scheme and time-temperature history rather than to the way mass transfer is described.

An important feature of the model is detailed treatment of the coupling between mass transfer processes and kinetics. Previous models utilize mass transfer coefficients which must be adjusted heuristically to account for the way the coupling influences the overall conversion. Here the interactions are handled in terms of diffusion and bulk flow within the particle, processes which can be more directly related to structural properties of the particle. Nevertheless, the number of required parameters remains the same. Finally, the approach emphasizes the importance of mass transfer, describes how its influence can be separated from intrinsic kinetic processes, and suggests the sort of structural information required to understand short contact time pyrolysis and hydropyrolysis.

0001-1541-79-1897-0065-$01.75.

In hydropyrolysis, small coal particles are exposed to hot, high pressure hydrogen for a short time to produce gaseous and liquid products. Typical conditions include temperatures up to 1 100°C, hydrogen pressures to several hundred atmospheres, particles as small as 50 μ_m, and reaction times as short as 10^{-1} s. The short contact time process appears attractive because yields significantly exceeding the proximate volatiles content are possible. Products include light gases such as methane, ethane, and the oxides of carbon as well as benzene and its derivatives and heavier aromatic liquids. Anthony and Howard (1976) present a broad survey of the field.

While high yields are possible, several experimental studies (Anthony et al., 1976; Suuberg, Peters, and Howard, 1977; Graff et al., 1976; Steinberg and Fallon, 1975; Greene, 1977) demonstrate that both the overall yield and the product distribution are sensitive to several process variables: temperature, pressure, hydrogen partial pressure, particle size, reaction time, product residence time, and coal type. Observed trends suggest the influence of several interacting rate processes: heat transfer, devolatilization of the solid coal, both gas-solid and gas phase secondary reactions, mass transfer within the particle, and hydrogenation of the char. Optimal reactor design requires a model incorporating these or at least systematic correlations involving all the relevant variables. Reaction kinetics and heat transfer have received the most attention thus far. Mass transfer has been virtually ignored except in the MIT work (Anthony et al., 1976) which discloses that it may have a preeminent role.

The dramatic pressure dependence of weight loss for a bituminous coal suggested the presence of resistance to the escape of volatiles from a decomposing coal particle. In the MIT model, this resistance was lumped into a necessarily ambiguous external film coefficient. In addition, a fraction of the volatiles was assumed to deposit as char if retained within the particle, providing a competitive effect to account for the reduced yields at high pressures where deposition would be relatively fast. The authors avoided speculation about the internal structure of the particle during reaction and did not identify the mode of mass transfer. While the model correlated data for a single particle size fairly well, it did not explain the sharp increase in yield observed with decreasing particle size.

In this paper, we analyze in detail mass transfer within a single coal particle in order to elucidate these trends in overall yield. Such a single-particle model provides information which can later be coupled into a large scale reactor model. At this point, the particle is assumed to remain a porous sphere during decomposition, with mass transport occurring through diffusion and hydrodynamic flow. This idealization provides a well-defined basis for the model but may not be applicable to some plastic coals.

Analyses of diffusion and reaction in catalyst pellets (Aris, 1975), although possessing several similarities to our model, are not directly applicable to hydropyrolysis for two reasons. First, during the transient decomposition, the reaction rates (and possibly the physical structure) change rapidly, in contrast to the slowly varying conditions of most catalytic processes. Second, devolatilization drives a significant hydrodynamic flow out of the coal particle, whereas catalytic conversions frequently approximate equimolar counterdiffusion.

On the chemical side of the picture, we employ the weight loss kinetics of Anthony et al. (1976) which identify five species: reactive coal, activated coal, reactive volatiles, stable volatiles, and hydrogen. Even with this simplification, the conservation equations comprise an intractable set of coupled nonlinear partial differential equations. By estimating the time scales for the individual rate processes, however, a tractable and meaningful model can be formulated. The key lies in the rates of bulk flow and stabilization of the reactive volatiles by hydrogen, both of which are rapid relative to devolatilization.

This disparity of time scales allows two significant simplifications. First, the concentration and pressure profiles quickly equilibrate to the changing devolatilization rate, permitting description of the internal processes in terms of a pseudo-steady state and eliminating an explicit time-dependence from the conservation equations. Second, if the stabilization reaction is treated as being essentially instantaneous, the coexistence of hydrogen and reactive volatiles is precluded. Thus, the number of components is reduced locally by one, and the particle interior divides into two regions: a sheath accessible to diffusing hydrogen and containing no reactive volatiles, and a core devoid of hydrogen. The instantaneous yield of volatiles then depends strongly on the size of the core and the rate of deposition within it.

This model resembles the diffusion-controlled combustion of pulverized coal for which Nusselt (1916) developed the "shrinking core" model for diffusion of oxygen through a sheath of ash to the reactive carbon. With the assumptions of instantaneous oxidation and pseudo steady concentration profile, Nusselt's theory predicts the rate at which the combustion interface, initially at the external surface, burns toward the center as the reaction consumes carbon. The uniform production of volatiles characteristic of hydropyrolysis and their outward flow have no counterparts in this model, so the similarities remain qualitative.

The next two sections are devoted to development of the model; several order of magnitude arguments are presented to motivate the various approximations. The solutions derived in the third section pertain to slow devolatilization, wherein hydrogen permeates the entire particle and no core exists. Then the concentration profiles and core size for rapid devolatilization are calculated in terms of the pressure and particle size. These results lead to the instantaneous volatiles yields discussed in the fifth section. Several analytical results for limiting cases illustrate the physics, while numerical solutions cover the entire range of parameters. The predicted variations in yield with pressure, hydrogen partial pressure, and particle size agree qualitatively with available data.

In the sixth section we obtain the overall yield for hydropyrolysis by integrating the instantaneous values over the reaction time and adding the yield from the slower hydrogenation of char. To illustrate the interaction between kinetic processes and mass transfer clearly, the rate expression for devolatilization and the time-temperature history have been simplified by assuming a single first-order rate constant, instantaneous heatup, and a long reaction time. The integrated yield structure is qualitatively similar to the instantaneous yield.

Finally, we compare our predictions with the data of Anthony et al. (1976). With lignite, which shows no indication of softening, Anthony found no particle size dependence and only a modest effect of hydrogen, interpreted as the absence of reactive volatiles. While our theory will easily correlate these data, it provides no real test because mass transfer effects are unimportant. Therefore, we concentrate on the data for Pittsburgh No. 8 bituminous coal. First, three unknown parameters in our model (the same number as in the MIT model) are determined from their weight loss data, producing values which closely correspond to independent estimates from similar systems. The resulting theoretical curves conform to the data quite well, with variations in pressure, hydrogen partial pressure, and particle size, supporting to some

extent the transport model. Owing to our idealized devolatilization rate expression and time-temperature history, the effect of temperature in high pressure hydropyrolysis is poorly represented.

PHYSICAL AND CHEMICAL BASIS OF THE MODEL

Coal is a heterogeneous mixture of organic minerals of common botanical origin known as macerals, many of which have been identified by their physical properties but remain ill-defined chemically. Since a particular coal is a poorly characterized mixture of these macerals, the complete delineation of the chemical and physical processes involved in pyrolysis or hydropyrolysis seems remote. On the other hand, the integrated behavior of such processes, observed as carbon conversion or in terms of yields of individual chemical species, appears much simpler. The trends with variations in pressure and temperature suggest an interpretation based on a small number of chemical reactions and transport processes. In this section, we present the basic assumptions for a quantitative model of these interactions within an individual coal particle. Our idealization has been guided by careful ordering of the various rates and by experimental results.

The description of the chemistry follows closely the work of Anthony et al. (1976) which itself subsumed several earlier kinetic models. The new features introduced here lie not in these kinetics but in the detailed description of mass fluxes within an individual coal particle and the subsequent identification and evaluation of the relevant dimensionless groups in the conservation equations.

Chemical Kinetics

Our kinetic model consists of three sets of reactions: primary devolatilization, secondary deposition, and hydrogenation. If individual reactant and product species could be identified, each set would contain many reactions proceeding at different rates. Without detailed information, the reactants and products are lumped into the following categories: reactive coal, activated coal, inert char, stable volatiles, unstable volatiles, and hydrogen. The roles of these categories will become clearer in the discussion below. As more information on product distributions and the chemical structure of the coal as functions of the reaction conditions become available, further differentiation and sophistication will be possible. At this point, however, we settle for a kinetic model sufficient to explain variations in weight loss.

A convenient starting point is the thermal devolatilization of coal at sufficiently low pressures for secondary gas phase reactions and mass transfer effects to be negligible. Thermally induced rupture of chemical bonds releases hydrogen-rich volatiles, the product in gasification processes, and leaves a carbon-rich solid char. The evolution of volatiles can logically be modeled as a first-order process by analogy to the thermal decomposition of pure organic compounds. Ultimate yields and rate constants for many coals under a variety of conditions have been correlated on this basis, but an examination of these results reveals several shortcomings (Anthony and Howard, 1976). First, the ultimate yield for a particular coal depends on temperature and fails to correlate with the standard measurement of proximate volatile matter. Furthermore, the Arrhenius type of temperature dependence of the rate constant often produces activation energies far too low, ~ 8 to 80°K-J/mole, for organic decompositions. To compound the problem, at high temperature significant weight loss occurs in the initial 0.1 to 0.5 s in which the coal particle may be heating up at a rate dependent on the reactor configuration.

Anthony et al. (1976) resolved these difficulties for their data by implementing Vand's (1943) analysis of the decomposition in terms of a set of independent first-order reactions with a spectrum of activation energies and then integrating the rate over the experimental time-temperature history to obtain the yield. The approach seems plausible because the carbon-carbon and carbon-oxygen bound strengths in coal must vary widely with a corresponding distribution of activation energies. The temperature dependence of the ultimate yield can then be quantitatively explained as a kinetic effect due to the extremely slow rates at low temperatures of the reactions with high activation energies. The empirically determined distribution of activation energies characterized by only two adjustable parameters, the mean E_o and the standard deviation σ, correspond to those expected for organic decompositions (80 to 370 kJ/mole). To fit the same data with a single exponential requires a very low activation energy, ~ 40 to 60 kJ/mole.

With both the single and multiple reaction models, the primary devolatilization of reactive coal

$$C \xrightarrow{k_o} (1-\nu)V + \nu V^* + C^* \tag{1}$$

is first order in the reactive coal C with rate constant

$$k_o = \begin{cases} A_o e^{-E_o/RT} & \text{single reaction} \\ A_o \int_o^\infty f(E) e^{-E/RT}\, dE & \text{multiple reactions} \end{cases} \tag{2}$$

The differences between the two models surface only when the rate is integrated over the time-temperature history to obtain the yield for a finite reaction time. For low pressure pyrolysis, the reactive and unreactive volatiles are indistinguishable, and the activated coal C^* does not react further.

At higher pressures, the devolatilization yields for some coals, bituminous for example, show significant particle size and pressure dependence (Mazumdar and Chatterjee, 1973; Anthony and Howard, 1976). These are attributed to secondary reactions involving the unstable or reactive volatiles V^*, apparently associated with tarry, or higher molecular weight-species possibly evolved as free radicals. The nature of the reactions also remains unclear; some evidence supports polymerization of the tars followed by deposition as coke, while other experiments favor cracking to coke and gas. In either case, the reduction in yield depends on competition between the secondary reaction within the particle and the mass transfer process by which the volatiles escape to the surrounding gas. The extent of deposition, therefore, increases with increasing particle size and with increasing pressure. The former produces a longer residence time inside the particle, while the latter raises the molar density of volatiles and hence the deposition rate.

To accommodate these effects, Anthony and Howard distinguished between the reactive and unreactive volatiles as already indicated in (1) and introduced the deposition reaction

$$V^* \xrightarrow{k_1} S \tag{3}$$

with rate

$$k_1 \frac{p x_{v^*}}{RT}$$

In a hydrogen atmosphere, the volatile yield equals or exceeds that in an inert gas at the same temperature and pressure. Two complementary mechanisms appear to ex-

TABLE 1

A. Anthony and Howard (1976)

Devolatilization

$$C \xrightarrow{k_o} (1-\nu)V + \nu V^* + C^*$$

$$R_o = k_o C$$

Deposition

$$V^* \xrightarrow{k_1} S$$

$$R_1 = k_1 \frac{p}{RT} x_v^*$$

Stabilization

$$V^* + H_2 \xrightarrow{k_2} V$$

$$R_2 = k_2 \frac{p^2}{(RT)^2} x_{H_2} x_v^*$$

B. Moseley and Paterson (1965)

Direct hydrogenation

$$C^* + H_2 \xrightarrow{k_3} V + C^*$$

$$R_3 = k_3 \frac{p}{RT} C^* x_{H_2}$$

Polymerization

$$C^* \xrightarrow{k_4} S$$

$$R_4 = k_4 C^*$$

plain the enhancement. First, hydrogen reacts rapidly with organic free radicals (Benson, 1960) to form stable gas phase species, providing a mechanism for stabilizing the reactive volatiles according to the scheme

$$V^* + H_2 \xrightarrow{k_2} V \tag{4}$$

with rate

$$k_2 \frac{p^2}{(RT)^2} x_{v^*} x_{H_2}$$

and x_{H_2} the mole fraction of hydrogen. Second, the char remaining after partial devolatilization reacts with hydrogen to produce volatiles at a rate dependent upon the age of the char but much slower than the devolatilization. Moseley and Paterson (1965) proposed that active regions C^* produced by the primary devolatilization (1) can further react with hydrogen as

$$C^* + H_2 \xrightarrow{k_3} V + C^* \tag{5}$$

with rate $k_3 C^* p x_{H_2}/RT$ or disappear by a first-order thermal decomposition

$$C^* \xrightarrow{k_4} S \tag{6}$$

For slow decomposition relative to the devolatilization, the concentration of active sites decays from the total available C_o^* as

$$C^* = C_o^* e^{-k_4 t} \tag{7}$$

producing a volatile yield from direct hydrogenation of

$$\frac{k_3 C_o^*}{k_4 RT} p x_{H_2} (1 - e^{-k_4 t}) \tag{8}$$

For reaction times long relative to k_4^{-1}, the yield asymptotes to a constant proportional to the hydrogen pressure. More complex models capable of fitting a wider range of experimental data have been proposed by Zahradnik and Glenn (1971) and Johnson (1974), but the above theory satisfies our present needs.

The reactions described above, along with the appropriate rate expressions, comprise our kinetic model. The stoichiometry and rates for the four primary components (reactive coal, stable volatiles, unstable volatiles, and hydrogen) are summarized in Table 1. We now proceed to formulate expressions for the fluxes which transport the volatile products out of the particle.

Transport Processes

Both heat and mass transfer affect the volatiles yield from pyrolysis and hydropyrolysis. In the kinetic picture described above, mass transfer enters through both the escape of reactive volatiles from the particle and the intrusion of hydrogen to stabilize the reactive volatiles or react with the active solid. The time-temperature history of the particle, which influences the balance between kinetic and mass transfer effects, is determined not only by the environmental temperature but also by the thermal response of the particle and the energy released by reaction. A discussion of both of these rate processes must begin with the physical structure of the coal particle, itself a complex and incompletely understood subject. After describing a simplified structural model, we present the mass transfer mechanisms in detail. Then the relevant aspects of the heat transfer process are summarized.

The physical transformations of a coal particle exposed to an elevated temperature depend strongly on its initial composition as well as the environmental conditions. Two limiting cases are well defined. Certain coals maintain a porous structure throughout devolatilization, ultimately leaving a fragile skeleton of ash and char. Plastic coals, on the other hand, apparently soften into a droplet from which volatiles may escape as bubbles until resolidification occurs. While no absolutely reliable means of differentiation exists, the plasticity, or swelling, correlates fairly well with both volatile matter and carbon content (Loison et al., 1963) for measurements at 1 atm of inert gas and low heating rates, $\sim 10^{-2}$ to 2×10^{-1} °C/s. Swelling occurs for volatile contents of 15-40% and carbon contents of 81 to 92% with maxima near 30 and 89%, respectively. Lignites and anthracites fall outside these ranges, while low volatile bituminous coals generally exhibit the most marked plasticity.

These test conditions do not correspond, however, to process conditions for flash hydropyrolysis, leaving the relevant physical structure uncertain. Several experiments indicate that softening becomes more pronounced with higher pressures, higher heating rates, and hydrogen atmospheres (Loison et al., 1963), but the extrapolation to conditions of interest is tenuous. In addition, evidence on the effect of particle size is ambiguous, with little data available on individual particles in the 100 μm range.

Here we choose to model the coal particle as a porous sphere which more or less retains its integrity as the reaction proceeds. The initial internal structure apparently consists of both macro and micropore systems as indicated by low temperature adsorption and heat of wetting measurements (Van Krevelen, 1961). The 10^{-4}-10^{-3} μm dimensions of the smaller pores, however, severely limit diffusion of even small molecules; thus, for processes with time scales of a minute or less, these regions should be relatively inaccessible. The pore structure in our model is characterized, therefore, by a single size, corresponding to the macropores.

Although the model will fail if the pores close immediately, it retains its validity as long as some semblance of open structure remains during the evolution of reactive volatiles. Here the model will be tested indirectly by comparing predictions with experimental results. Data on particle structure during the evolution of volatiles under relevant process conditions would be extremely useful.

For a porous coal particle, mass transport resembles that encountered in porous catalyst pellets but with two significant differences. First, devolatilization generates large volumes of gas, thereby driving a significant bulk flow. Catalytic conversions, on the other hand, generally approximate equimolar counterdiffusion with negligible effect of volume change. Second, the decomposition is inherently transient, with both the rate of volatile evolution and the particle structure changing over the reaction time. We present general flux relations capable of handling these complexities in this section and in the next analyze the time scales characterizing the various transients.

Simple flux expressions including both multicomponent diffusion and bulk flow can be derived from the dusty gas model of Mason et al. (1967). Hite and Jackson (1977) discuss the application of this model to the catalyst problem, elucidating several limiting cases. Although the theory has a wide range of validity, extending from the continuous range down to pore sizes comparable to the mean free path of the gas molecules, this generality is unnecessary for our purposes, since the macropore dimensions of ~0.01 to 1.0 μm (Van Krevelen, 1961; Wen/Dutta et al., 1975) generally exceed the mean free path. The mean free path for small molecules such as carbon dioxide and methane at 1 000°K, for example, ranges from 10^{-1} μm at 1 atm to 10^{-3} μm at 100 atm. For mixtures of larger molecules, the paths should be shorter. Therefore, we take the continuum limit of the theory and obtain relations between the molar fluxes with respect to fixed coordinates N_i and the radial gradients in the mole fractions x_i and the pressure p:

$$\sum_{\substack{j=1\\ j\neq 1}}^{n} \frac{x_j N_i - x_i N_j}{D^e_{ij}} = -\frac{p}{RT}\frac{dx_i}{dr} - \frac{x_i}{RT}\left[1 - \frac{1}{\sum_{j=1}^{n} x_j (M_j/M_i)^{1/2}}\right]\frac{dp}{dr} \quad (9)$$

Only $n-1$ of these equations are independent; the final equation characterizes the bulk flux; namely

$$\sum_{j=1}^{n} M_j^{1/2} N_j = -\frac{B_o p}{\mu RT}\sum_{j=1}^{n} M_i^{1/2} x_j \frac{dp}{dr} \quad (10)$$

Note that if all species have the same molecular weight, the last term in (9) vanishes, we obtain the Stefan-Maxwell equations (Hirschfelder, Curtis, and Bird, 1954), and (10) becomes Darcy's law in its familiar form.

The physical properties appearing in (9) and (10) deserve further comment. The effective diffusivity D^e_{ij} is related to the binary diffusivity D_{ij} by a geometrical factor K_1 (dependent on the structure but not the pore size) as

$$D^e_{ij} = K_1 D_{ij}, \quad K_1 << 1 \quad (11)$$

Since $D_{ij} \propto 1/p$ (Reid and Sherwood, 1958), the product pD_{ij} will be treated as a constant. The Darcy permeability B_o also depends on the structure and is proportional to the square of the pore size; both B_o and K_1 can be estimated from porosity and surface measurements (Scheidegger, 1960; Aris, 1975). Variations in K_1 and B_o with extent of reaction and μ and D_{ij} with gas composition will be ignored for the moment.

The intrusion of hydrogen and the escape of volatiles from the porous particle might also be limited by transport in the external gas. For pure diffusion with no bulk flow

$$\frac{\text{external conductance}}{\text{internal conductance}} = \frac{D_{ij}/a}{D^e_{ij}/a} = \frac{1}{K_1} \quad (12)$$

indicating that the internal resistance dominates except for extremely porous particles, where $K_1 \sim 0(1)$. The bulk flow of volatiles reduces the conductances for hydrogen below these values by an amount proportional to the linear velocity. Conservation of mass, however, requires the velocity to be greater within the pores, where the cross section for flow is smaller. Hence, the internal conductance decreases faster than the external, further increasing the ratio given by (12). Similarly, convection of the bulk gas past the particle increases the external conductance without affecting the internal, again increasing their ratio. We conclude, therefore, that for a devolatilizing coal particle internal mass transfer resistances dominate, in accord with similar analyses of catalyst pellets (Hutchings and Carberry, 1966).

Three sorts of processes are involved in establishing the temperature of a coal particle: conduction and convection to the particle's outer surface, conduction and bulk flow inside the particle, and energy absorption and evolution due to the various reactions. In situations where a small particle is exposed to a high temperature gas, the heatup rate is characterized by the natural time scales of the internal and external processes. The time scale for heatup when the external resistance controls is $a(\rho c_p)_s/h$; $(\rho c_p)_s$ is the volumetric heat capacity of the particle, and h the external heat transfer coefficient. Inside the particle, the time scale for conduction is a^2/α_s. These two time scales are roughly the same order of magnitude, about 10^{-2} s for 100 μm particles at 600°C, disclosing that both external and internal processes are important in establishing the thermal response of the particle. Bulk flow, on the other hand, plays a very minor role. Heat transfer by bulk flow can be compared to the flux due to conduction in terms of the ratio

$$\frac{k_o C_o RT}{p_o}\frac{a^2(\rho c_p)_g}{\alpha_s(\rho c_p)_s} = \frac{\text{(transfer by bulk flow)}}{\text{(conduction)}} \quad (13)$$

which is small (10^{-4}-10^{-2}) for particles 100 μm and smaller. For larger particles (about 1 000 μm), the ratio increases to become 0(1) at roughly 100 atm.

When the time scales for devolatilization and hydrogenation are slower than conduction for small particles (about 100 μm), internal temperature gradients can be ignored. With reactions involving oxygen, water, and the oxides of carbon, on the other hand, there may be significant thermal effects, especially in hydropyrolysis. For the present, however, these have been omitted.

In its present stage of development, then, the model treats the particle as though it were spatially isothermal. Furthermore, in studies to be described later on rapid heatup, temporal variations are suppressed.

Conservation Equations

Using the reaction rates and fluxes from the preceding two sections, we can formulate the conservation equations for the four gaseous species: reactive and unreactive vola-

tiles, hydrogen, and inert gas. This means four equations of the form

$$\frac{\partial}{\partial t}\frac{px_i}{RT} + \frac{1}{r^2}\frac{\partial}{\partial r} r^2 N_i = R_i \qquad (14)$$

with

$$c_i = c_i^B \quad \text{at} \quad r = a$$
$$x_i = x^o_i \quad \text{at} \quad t = 0 \qquad (15)$$

and suitable initial conditions. Rather than attempt to solve this set of coupled, nonlinear partial differential equations directly, we have analyzed the time scales characterizing the various rate processes and capitalized on the disparities among them to greatly simplify the mathematics.

The problem contains six independent time scales: one each for diffusion and bulk flow plus four for the chemical reactions. Estimates of the time scales for all but the deposition reaction, which is not controlling, are given in Table 2. Those for devolatilization and hydrogenation are based on Anthony and Howard's (1976) bituminous data (Figures 1 and 12 in their review). The time constants for stabilization pertain to methyl and ethyl radicals (Benson, 1960, pp. 296, 299) and are somewhat more speculative. The physical properties used in the calculations of the transport processes

$$K_1 \sim \frac{\phi}{\tau} \sim 10^{-1} \qquad p_o D_{ij} \sim 10^{-5}\ \frac{\text{atm}\cdot\text{m}^2}{\text{s}}$$

$$B_o \sim K_1 d^2 \sim 10^{-15}\text{m}^2 \qquad Pr \sim 0.6$$

$$(\rho c_p)_s \sim 4 \times 10^5\ \frac{J}{\text{m}^3\text{-}^\circ\text{K}} \qquad \mu_o \sim 10^{-5}\ \text{Pa}\cdot\text{s} \qquad (16)$$

correspond to gases in the 600° to 1 000°C range (Reid and Sherwood, 1958) and porous materials with void volume $\phi \sim 0.2$ to 0.3, pore diameters $d \sim 0.1$ μm, and thermal properties from Badzioch et al. (1964). Despite the inherent uncertainty in these estimates, several clear conclusions can be drawn.

One must recognize that the devolatilization rate sets the relevant time scale against which the others should be measured. On this basis, bulk flow and the stabilization of free radicals with hydrogen are generally much faster, while diffusion and direct hydrogenation are slower. This ordering permits two major simplifying assumptions.

First, the volatiles clearly cannot escape by diffusion alone, except for very small particles at reduced pressures, but their flux can easily be accommodated by bulk flow. Indeed, the pressure difference required for the latter should only be a small fraction of the external pressure, allowing a linearization in the flux relations (9) and (10). Furthermore, the flow should equilibrate instantaneously with changing devolatilization rate, permitting a pseudo-steady description of the concentration profiles.

Second, hydrogen stabilizes reactive volatiles much more rapidly than it diffuses through the particle, except in small particles at low pressures. Hence, this reaction will be assumed to be instantaneous, so that hydrogen and reactive volatiles do not coexist. Instead, reactive volatiles released in a hydrogen-rich region will be immediately stabilized, while those evolved in a hydrogen-free region will flow to an interface where the hydrogen flux can sustain the reaction and both concentrations vanish. As a consequence, each region contains only three components.

TABLE 2. ESTIMATES OF TIME SCALES

Chemical reactions	600°C	1 000°C
Devolatilization	1 sec	10^{-1}
Hydrogenation	10	1
Stabilization of free radicals	10^{-2}	10^{-3}

	1 atm		100 atm	
Transport processes*	10^2 μm	10^3 μm	10^2 μm	10^3 μm
Diffusion				
a^2/D_{eff}	10^{-3} s	10^{-1}	10^{-1}	10
Bulk flow				
$\mu a^2/pB_o$	10^{-3}	10^{-1}	10^{-5}	10^{-3}
Energy				1
$\alpha(\rho c_p)_s/h$	10^{-3}	1	10^{-2}	1
a^2/a_s	10^{-3}	1	10^{-2}	

* At 600°C.

The stabilization reaction should be distinguished from hydrocracking of reactive volatiles which proceeds slowly by comparison. Furthermore, the latter reaction should have little or no effect on weight loss.

Although the diffusivities of the components in each region are not equal, the differences will be suppressed for the present. This provides a simple qualitative description of the diffusion process and can be refined later, if necessary.

Our concept of hydropyrolysis of an individual coal particle can be summarized as follows. For slow rates of devolatilization, hydrogen permeates the entire particle, immediately stabilizing all reactive volatiles and thereby preventing deposition. Since all volatiles ultimately escape, the fractional yield is unity. Increases in the devolatilization rate reduce the hydrogen level within the particle, with the concentration at the center eventually falling to zero. A further increase above this critical value then produces a core depleted of hydrogen and bounded by the reaction interface described above (Figure 1); the associated reduction in yield due to deposition of reactive volatiles is proportional to the volume of the core and the deposition rate. At extremely high rates of devolatiliza-

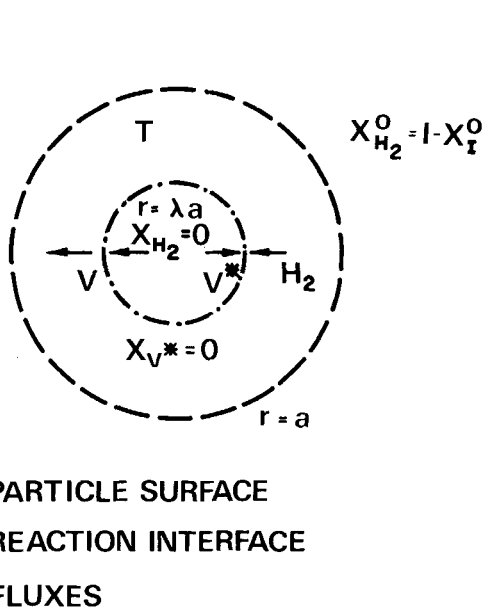

Fig. 1. Schematic of particle for rapid devolatilization with core depleted of hydrogen.

tion, bulk flow effectively excludes hydrogen from the particle, and the reaction interface coincides with the external surface. In the next section, we employ these concepts to simplify the conservation equations.

GOVERNING EQUATIONS

Our model is formulated using the following assumptions motivated by the preceding order of magnitude estimates:

1. Spatially isothermal particle.
2. No external mass transfer resistance.
3. Diffusion slow relative to bulk flow.
4. Pseudosteady pressure and concentration profiles.
5. Small increase in internal pressure.
6. Two regions separated by reaction interface at which hydrogen and reactive volatiles combine instantaneously.
7. Equal binary diffusivities; that is, $D^e_{ij} = D_{\text{eff}}$ for all i and j.

The flux relations for a ternary mixture satisfying assumptions 3, 4, 5, and 7 are

$$N_i = -\frac{p_o D_{\text{eff}}}{RT}\frac{dx_i}{dr} + x_i(N_1 + N_2) \tag{17}$$

and

$$\sum_{j=1}^{2} M_j^{1/2} N_j = -\frac{B_o p_o}{\mu RT}\sum_{j=1}^{3} M_j^{1/2} x_j \frac{dp}{dr} \tag{18}$$

The flux of component 3, the inert gas, does not appear since it must be zero at steady state. Note that the diffusive fluxes now resemble Fick's law for a binary mixture, but the bulk flow differs from Darcy's law in the molecular weight dependence. The latter difference proves unimportant because we never need to solve the third equation for the pressure.

It is worthwhile to identify the dimensionless groups characterizing the model. Our assumption that the stabilization reaction is instantaneous removes one characteristic time scale; comparing the devolatilization time to each of the other four produces

$$\begin{aligned}
\pi &= \frac{k_1 p_o}{k_o C\,RT} && \frac{\text{devolatilization}}{\text{deposition}} \\
\alpha^2 &= \frac{a^2 k_o C\,RT}{p_o D_{\text{eff}}} && \frac{\text{diffusion}}{\text{devolatilization}} \\
\epsilon &= \frac{a^2 \mu k_o C\,RT}{p_o^2 B_o} && \frac{\text{bulk flow}}{\text{devolatilization}} \\
\beta &= \frac{k_3 C_o^* p_o}{k_o C\,RT} && \frac{\text{devolatilization}}{\text{direct hydrogenation}}
\end{aligned} \tag{19}$$

where C is the molar density of volatiles in the particle. These parameters can also be interpreted as the dimensionless pressure π, the dimensionless particle size α, and the fractional increase in internal pressure ϵ. The order of magnitude estimates indicate that ϵ, β, and α^{-1} should be small; π, however, may vary throughout a wide range.

With the dimensionless variables

$$\begin{aligned}
\bar{p} &= \frac{p - p_o}{\epsilon p_o} \\
\bar{N}_i &= \frac{N_i}{a k_o C} \\
\bar{r} &= r/a
\end{aligned} \tag{20}$$

the conservation equations and fluxes for the two regions can be written as

(a) core

$$\begin{aligned}
\frac{1}{\bar{r}^2}\frac{d}{d\bar{r}}\bar{r}^2\bar{N}_v &= 1 - \nu \\
\frac{1}{\bar{r}^2}\frac{d}{d\bar{r}}\bar{r}^2\bar{N}_{v^*} &= \nu - \pi x_{v^*}
\end{aligned} \tag{21}$$

$$\begin{aligned}
\bar{N}_v &= -\alpha^{-2}\frac{dx_v}{d\bar{r}} + x_v(\bar{N}_v + \bar{N}_{v^*}) \\
\bar{N}_{v^*} &= -\alpha^{-2}\frac{dx_{v^*}}{d\bar{r}} + x_{v^*}(\bar{N}_v + \bar{N}_{v^*})
\end{aligned} \tag{22}$$

$$\begin{aligned}
\bar{N}_v + \left(\frac{M_{v^*}}{M_v}\right)^{1/2}\bar{N}_{v^*} = \\
-\left(\frac{M_I}{M_v}\right)^{1/2}\left\{1 - \left[1 - \left(\frac{M_v}{M_I}\right)^{1/2}\right]x_v \right. \\
\left. - \left[1 - \left(\frac{M_{v^*}}{M_I}\right)^{1/2}\right]x_{v^*}\right\}\frac{d\bar{p}}{d\bar{r}}
\end{aligned} \tag{23}$$

(b) sheath

$$\begin{aligned}
\frac{1}{\bar{r}^2}\frac{d}{d\bar{r}}\bar{r}^2\bar{N}_v &= 1 + \beta x_{H_2} \\
\frac{1}{\bar{r}^2}\frac{d}{d\bar{r}}\bar{r}^2\bar{N}_{H_2} &= -\nu - \beta x_{H_2}
\end{aligned} \tag{24}$$

$$\begin{aligned}
\bar{N}_v &= -\alpha^{-2}\frac{dx_v}{d\bar{r}} + x_v(\bar{N}_v + \bar{N}_{H_2}) \\
\bar{N}_{H_2} &= -\alpha^{-2}\frac{dx_{H_2}}{d\bar{r}} + x_{H_2}(\bar{N}_v + \bar{N}_{H_2})
\end{aligned} \tag{25}$$

$$\begin{aligned}
\bar{N}_v + \left(\frac{M_{H_2}}{M_v}\right)^{1/2}\bar{N}_{H_2} = \\
-\left(\frac{M_I}{M_v}\right)^{1/2}\left\{1 - \left[1 - \left(\frac{M_v}{M_I}\right)^{1/2}\right]x_v \right. \\
\left. - \left[1 - \left(\frac{M_{H_2}}{M_I}\right)^{1/2}\right]x_{H_2}\right\}\frac{d\bar{p}}{d\bar{r}}
\end{aligned} \tag{26}$$

Associated with these are three sets of boundary conditions.

1. The fluxes must satisfy the usual regularity conditions at the origin:

$$\lim_{\bar{r}\to 0}\bar{r}^2\bar{N}_i = 0 \tag{27}$$

2. At the reaction interface $\bar{r} = \lambda$, the hydrogen and reactive volatiles concentrations must be zero

$$x_{H_2} = x_{v^*} = 0 \tag{28}$$

and the fluxes must balance as

$$\begin{aligned}
\bar{N}_{H_2}(\lambda^+) &= -\bar{N}_{v^*}(\lambda^-) \\
\bar{N}_v(\lambda^+) &= \bar{N}_v(\lambda^-) + \bar{N}_{v^*}(\lambda^-)
\end{aligned} \tag{29}$$

3. The compositions and pressure must match those of the bulk gas at $\bar{r} = 1$:

$$\bar{p} = 0$$
$$x_{H_2} = x^o_{H_2} \qquad (30)$$
$$x_v = x_{v^*} = 0$$

The position of the reaction interface λ remains unknown, but will be determined by the interfacial conditions (28) and (29). In the next two sections we solve these equations, first for slow devolatilization with hydrogen permeating the entire particle, that is, $\lambda = 0$, and then for fast devolatilization with $\lambda > 0$.

SLOW DEVOLATILIZATION

For sufficiently slow rates of devolatilization, hydrogen can diffuse into the particle fast enough to overcome the bulk flow and stabilize all reactive volatiles. Indeed, this occurs whenever the parameter α, characterizing the ratio of the devolatilization rate to diffusion, falls below a certain critical value (determined below). For the present, we will ignore direct hydrogenation on the assumption that β is small.

The fluxes are obtained by integrating the conservation equations for the sheath (24) and applying the regularity conditions (27):

$$\bar{N}_v = \frac{1}{3}\bar{r}$$
$$\bar{N}_{H_2} = -\frac{1}{3}\nu\bar{r} \qquad (31)$$

These solutions, the flux relations (25), and the boundary conditions at the outer surface (30) then determine the concentration profiles

$$x_v = \frac{1}{1-\nu}\left\{1 - \exp\left[-\frac{1-\nu}{6}\alpha^2(1-\bar{r}^2)\right]\right\}$$
$$x_{H_2} = \left[x^o_{H_2} + \frac{\nu}{1-\nu}\right] \exp\left[-\frac{1-\nu}{6}\alpha^2(1-\bar{r}^2)\right] - \frac{\nu}{1-\nu} \qquad (32)$$
$$x_I = (1 - x^o_{H_2}) \exp\left[-\frac{1-\nu}{6}\alpha^2(1-\bar{r}^2)\right]$$

Even without reactive volatiles, gradients exist because of the competition between bulk flow and diffusion. Their presence, that is, $\nu > 0$, sharpens the concentration gradients through the consumption of hydrogen by the stabilization reaction.

The fractional rate of volatile evolution, the yield, is

$$\eta_v = \frac{4\pi a^2 N_v|_{r=a}}{\frac{4\pi a^3}{3}k_o C} = 1 \qquad (33)$$

which is no surprise, since instantaneous stabilization by hydrogen throughout the particle prevents any deposition of reactive volatiles.

From (19) and (32), it is evident that an increase in the devolatilization rate relative to diffusion increases α and reduces the hydrogen concentration in the interior of the particle. When the minimum concentration at $\bar{r} = 0$ falls below zero, this solution becomes invalid owing to the formation of a hydrogen free core. The corresponding critical value of α follows from (32), with $x_{H_2} = \bar{r} = 0$, as

$$\alpha^2_{crit} = \frac{6}{1-\nu}\ln\left(1 + \frac{1-\nu}{\nu}x^o_{H_2}\right) \qquad (34)$$

Under pyrolysis conditions, $x^o_{H_2} = 0$ and $\alpha_{crit} = 0$, so a core always exists. Without reactive volatiles $\nu = 0$, $\alpha_{crit} \to \infty$ and there is, of course, no core. Whenever $x^o_{H_2} \sim 0(1)$, α^2_{crit} will be considerably greater than one, a fact which will be exploited in the next section when we analyze the case of $\alpha > \alpha_{crit}$.

RAPID DEVOLATILIZATION

When $\alpha > \alpha_{crit}$, the slow diffusion of hydrogen into the particle limits the yield of volatiles. In this section, the precise reduction in yield is calculated by integrating the conservation equations for the core and sheath, subject to the boundary conditions mentioned earlier, to determine the concentration profiles and the position of the reaction interface. In the process, we must assume that $\alpha^2 >> 1$.

Equations (21) and (22) together with the boundary conditions at the origin (27) and at the reaction interface (28) and (29) determine the volatiles concentration in the core. A single integration of (21) produces

$$\bar{N}_v = \frac{1}{3}(1-\nu)\bar{r} \qquad (35)$$

but for the reactive volatiles (21), (22), and (35) combine into a nonlinear differential equation without an obvious analytical solution. For slow diffusion ($\alpha^2 >> 1$), however, an asymptotic solution can be derived by dividing the core into two regions: an interior dominated by bulk flow and a thin diffusion boundary layer at the reaction interface. Analytical solutions for these regions can then be matched asymptotically as shown below.

First, diffusion can be neglected in the interior of the core so

$$\bar{N}_{v^*} = \frac{x_{v^*}}{1-x_{v^*}}\bar{N}_v \qquad (36)$$

and from the conservation equation for reactive volatiles

$$\frac{1}{3}\bar{r}(1-\nu)\frac{d}{d\bar{r}}\frac{x_{v^*}}{1-x_{v^*}} + (1-\nu)\frac{x_{v^*}}{1-x_{v^*}} + \pi x_{v^*} = \nu \qquad (37)$$

Fortunately, the constant solution

$$x^c_{v^*} = \frac{1+\pi}{2\pi}\left[1 - \left(1 - \frac{4\nu\pi}{(1+\pi)^2}\right)^{1/2}\right] \qquad (38)$$

matches with the boundary-layer solution. Note that at low pressures, that is, $\pi << 1$, deposition is negligible, and $x^c_{v^*} \sim \nu$; when $\pi >> 1$

$$x^c_{v^*} \sim \frac{\nu}{\pi} \qquad (39)$$

indicating almost complete deposition in the core.

Transition from the finite interior concentration of reactive volatiles to zero at the reaction interface occurs through a boundary layer of thickness α^{-2}. Within this region the total flux remains constant, but the large gradients make diffusion competitive with bulk flow. The rescaled distance

$$y = \alpha^2(\lambda - \bar{r}) \sim 0(1) \qquad (40)$$

transforms (24) and (25) into

$$\frac{d}{dy}\bar{N}_{v^*} = \frac{d}{dy}\bar{N}_v = 0(\alpha^{-2}) \qquad (41)$$

and

$$\overline{N}_{v^*} = -\frac{dx_{v^*}}{dy} + x_{v^*}(\overline{N}_v + \overline{N}_{v^*})$$

$$\overline{N}_v = -\frac{dx_v}{dy} + x_v(\overline{N}_v + \overline{N}_{v^*}) \tag{42}$$

with $x_{v^*} = 0$ at $y = 0$. In addition to satisfying these equations, the boundary-layer solutions must match asymptotically as $y \to \infty$, with the limits of the interior solutions as $\bar{r} \to \lambda$. Thus, with negligible devolatilization or deposition in the thin layer, the fluxes remain constant

$$\overline{N}_{v^*} = \frac{1}{3}\lambda x^c{}_{v^*}\frac{1-\nu}{1-x^c{}_{v^*}}$$

$$\overline{N}_v = \frac{1}{3}\lambda(1-\nu) \tag{43}$$

and the mole fractions must satisfy

$$\frac{dx_{v^*}}{dy} + \frac{\lambda}{3}\frac{1-\nu}{1-x^c{}_{v^*}}x_{v^*} = \frac{\lambda\nu}{3}\left(1 - \pi\frac{x^c{}_{v^*}}{\nu}\right)$$

$$\frac{dx_v}{dy} + \frac{\lambda}{3}\frac{1-\nu}{1-x^c{}_{v^*}}x_v = \frac{\lambda}{3}(1-\nu) \tag{44}$$

The final solutions are

$$x_{v^*} = \nu\left(1 - \pi\frac{x^c{}_{v^*}}{\nu}\right)\frac{1-x^c{}_{v^*}}{1-\nu}\left[1 - \exp\left(-\frac{\lambda}{3}\frac{1-\nu}{1-x^c{}_{v^*}}y\right)\right]$$

$$x_v = (1-x^c{}_{v^*})\left[1 - \left(1 - \frac{x^{\lambda}{}_v}{1-x^c{}_{v^*}}\right)\exp\left(-\frac{\lambda}{3}\frac{1-\nu}{1-x^c{}_{v^*}}y\right)\right] \tag{45}$$

where $x^{\lambda}{}_v$, the unknown fraction of volatiles at the interface, remains to be determined by matching with the sheath solution.

Solution of the sheath equations without direct hydrogenation is also straightforward. One integration of (24) and application of the flux conditions (29) at $\bar{r} = \lambda$ produces

$$\overline{N}_v = \frac{1}{3}\bar{r} - \frac{1}{3}\pi x^c{}_{v^*}\frac{\lambda^3}{\bar{r}^2}$$

$$\overline{N}_{H_2} = -\frac{1}{3}\nu\bar{r} + \frac{1}{3}\pi x^c{}_{v^*}\frac{\lambda^3}{\bar{r}^2} \tag{46}$$

The two terms in $\overline{N}_v$ correspond to the total devolatilization minus the deposition in the core. The hydrogen flux balances the outward flux of reactive volatiles escaping the core, $\lambda^3(\nu - \pi x^c{}_{v^*})/3$, plus those evolved in the sheath, $(1-\lambda^3)\nu/3$.

Substitution of (46) into the flux relations (25) provides two differential equations for x_v and x_{H_2} with solutions

$$x_v = c_1 e^{\alpha^2(1-\nu)\bar{r}^2/6} + \frac{1}{1-\nu} - g\left[\left(\frac{1-\nu}{6}\right)^{1/2}\alpha\bar{r}\right]$$

$$x_{H_2} = c_2 e^{\alpha^2(1-\nu)\bar{r}^2/6} - \frac{\nu}{1-\nu} + g\left[\left(\frac{1-\nu}{6}\right)^{1/2}\alpha\bar{r}\right] \tag{47}$$

where

$$g(x) = \frac{\pi\lambda^3\alpha^3}{3}\left[\frac{(1-\nu)}{6}\right]^{1/2} x^c{}_{v^*}\left\{\frac{1}{x} + \sqrt{\Pi}\, e^{x^2}\operatorname{erf} x\right\} \tag{48}$$

where $\Pi = 3.14159\ldots$. These expressions are generally valid, unlike the approximate core solutions which were restricted to $\alpha >> 1$. From the boundary conditions at the outer surface (30)

$$c_1 = \left\{g\left[\left(\frac{1-\nu}{6}\right)^{1/2}\alpha\right] - \frac{1}{1-\nu}\right\} e^{-\alpha^2(1-\nu)/6}$$

$$c_2 = \left\{x^o{}_{H_2} + \frac{\nu}{1-\nu} - g\left[\left(\frac{1-\nu}{6}\right)^{1/2}\alpha\right]\right\} e^{-\alpha^2(1-\nu)/6} \tag{49}$$

while from the continuity condition at the reaction interface

$$x^{\lambda}{}_v = x_v|_{\bar{r}=\lambda^+} = \left\{g\left[\left(\frac{1-\nu}{6}\right)^{1/2}\alpha\right] - \frac{1}{1-\nu}\right\} e^{\alpha^2(1-\nu)(\lambda^2-1)/6} + \frac{1}{1-\nu} - g\left[\left(\frac{1-\nu}{6}\right)^{1/2}\alpha\lambda\right] \tag{50}$$

Now all constants have been determined except λ, the position of the reaction interface.

The final step is to require that

$$x_{H_2} = 0 \quad \text{at} \quad \bar{r} = \lambda \tag{51}$$

and thereby fix λ. The resulting nonlinear equation for λ

$$0 = \left\{x^o{}_{H_2} + \frac{\nu}{1-\nu} - g\left[\left(\frac{1-\nu}{6}\right)^{1/2}\alpha\right]\right\} e^{\alpha^2(1-\nu)(\lambda^2-1)/6} + g\left[\left(\frac{1-\nu}{6}\right)^{1/2}\alpha\lambda\right] - \frac{\nu}{1-\nu} \tag{52}$$

must, in general, be solved numerically. In several limits, however, analytical solutions serve as checks on the numerical work and also demonstrate the physics clearly.

First, consider the large and small particle asymptotes. For the former with $\alpha^2(1-\nu) >> 1$, the error functions can be expanded as

$$\operatorname{erf} x = 1 - \frac{e^{-x^2}}{\sqrt{\Pi}x}\left(1 - \frac{1}{2x^2} + \frac{3}{4x^4} - \ldots\right) \tag{53}$$

reducing (52) to

$$1 + \frac{1-\nu}{\nu}x^o{}_{H_2} - \lambda^3\pi\frac{x^c{}_{v^*}}{\nu} - \left(1 - \pi\frac{x^c{}_{v^*}}{\nu}\right)e^{\alpha^2(1-\nu)(1-\lambda^2)/6} = 0 \tag{54}$$

The exponential dominates unless $\lambda \approx 1$, so that

$$\lambda \approx 1 - \frac{3}{\alpha^2(1-\nu)}\ln\frac{1 + \frac{1-\nu}{\nu}x^o{}_{H_2} - \pi\frac{x^c{}_{v^*}}{\nu}}{1 - \pi\frac{x^c{}_{v^*}}{\nu}} \tag{55}$$

showing that hydrogen barely intrudes into large particles. With decreasing particle size, the relative penetration increases until the core disappears (that is, $\lambda = 0$) at

$$\alpha^2 = \frac{6}{1-\nu}\ln\left(1 + \frac{1-\nu}{\nu}x^o{}_{H_2}\right) \tag{56}$$

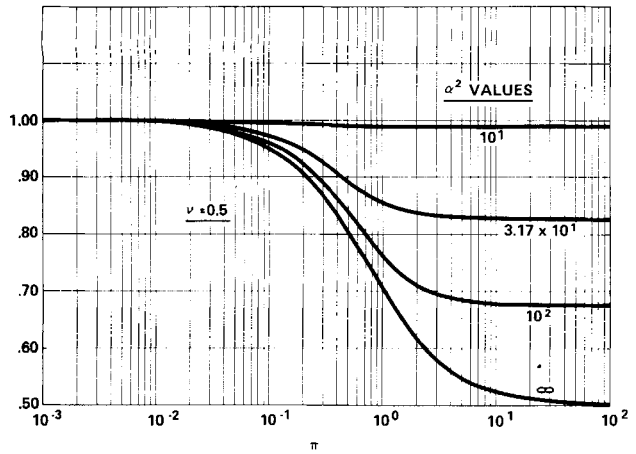

Fig. 2. Instantaneous yield of volatiles as function of dimensionless pressure π with α^2 (temperature and particle size) constant: ν = 0.5.

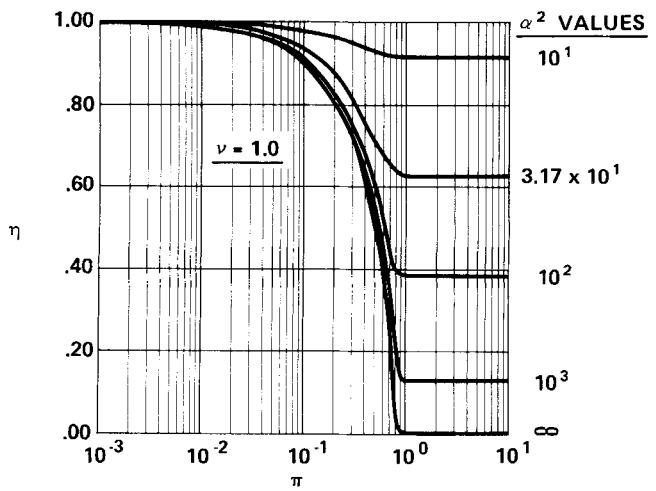

Fig. 3. Instantaneous yield of volatiles as function of dimensionless pressure π with α^2 (temperature and particle size) constant: ν = 1.0.

which agrees with α_{crit} (34) determined from slow devolatilization. With (54) we can also demonstrate the effect of pressure. For $\pi << 1$ and $\alpha^2(1-\nu) >> 1$, (54) becomes

$$1 + \frac{1-\nu}{\nu} x^o_{H_2} - e^{\alpha^2(1-\nu)(1-\lambda^2)/6} = 0 \qquad (57)$$

with the asymptotic solution

$$\lambda \sim 1 - \frac{3(1-\nu)}{\alpha^2} \ln\left(1 + \frac{1-\nu}{\nu} x^o_{H_2}\right) \qquad (58)$$

Recall that pressure affects only the deposition reaction. In this limit hydrogen must, therefore, diffuse against the maximum flux of volatiles, creating a core of maximum size corresponding to (58). Higher pressures increase deposition, thereby reducing the flux and allowing the core to shrink. For $\pi >> 1$, λ eventually asymptotes to a constant dependent only on α, $x^o_{H_2}$, and ν.

When the volatiles are all reactive, that is, $\nu = x^c_{v*} = 1$, expansion of (54) for $\alpha^2(1-\nu) << 1$ yields

$$\lambda^3 - \frac{1+2\pi}{2\pi}\lambda^2 + \frac{1 - 6(x^o_{H_2}/\alpha^2)}{2\pi} = 0 \qquad (59)$$

At low pressures

$$\lim_{\pi\to 0} \lambda = \left(1 - \frac{6x^o_{H_2}}{\alpha^2}\right)^{1/2} \approx 1 - \frac{3x^o_{H_2}}{\alpha^2} \qquad (60)$$

for $\alpha^2 >> 1$. When π exceeds 1, however, the solution (38) breaks down because all reactive volatiles in the core have deposited, and further pressure increases have no effect. Then the reaction interface is determined by

$$2\lambda^3 - 3\lambda^2 + 1 - \frac{6x^o_{H_2}}{\alpha^2} = 0 \qquad (61)$$

When $\alpha^2 >> 1$

$$\lambda \approx 1 - \left(\frac{2x^o_{H_2}}{\alpha^2}\right)^{1/2} \qquad (62)$$

again indicating a smaller core in the high pressure limit.

Finally, under pyrolysis conditions with $x^o_{H_2} = 0$, (52) can be satisfied only with $\lambda = 1$. Thus, reactive volatiles are preserved only by dilution in the external gas phase.

Next, the instantaneous yield of volatiles will be derived from these solutions and numerical results presented for a range of α, π, $x^o_{H_2}$, and ν.

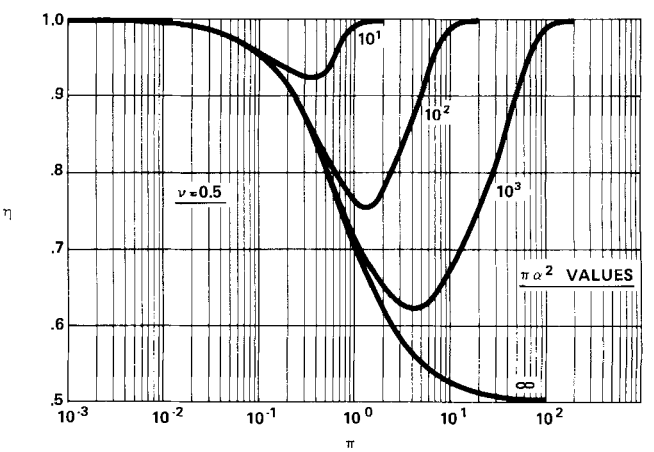

Fig. 4. Instantaneous yield of volatiles as function of dimensionless temperature π with $\pi\alpha^2$ (pressure and particle size) constant: ν = 0.5.

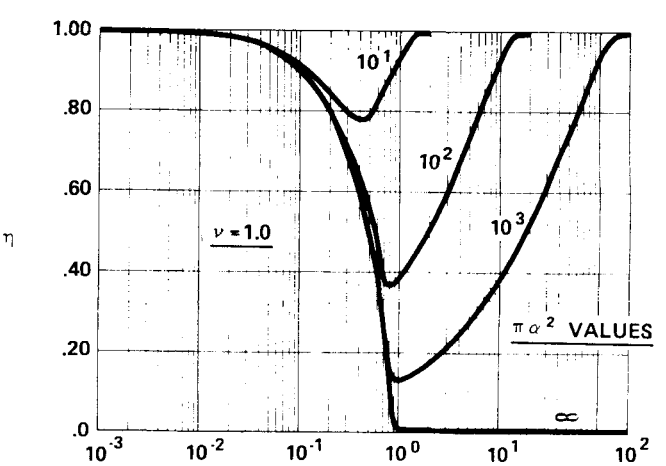

Fig. 5. Instantaneous yield of volatiles as function of dimensionless temperature π with $\pi\alpha^2$ (pressure and particle size) constant: ν = 1.0.

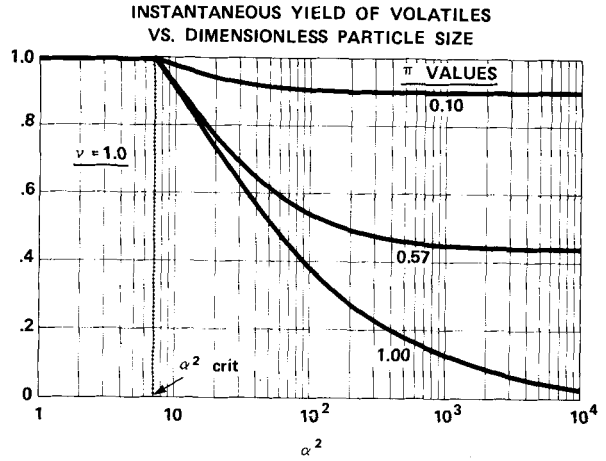

Fig. 6. Instantaneous yield of volatiles as function of dimensionless particle size α^2 with π (pressure and temperature) constant (ν = 1.0).

CALCULATION OF INSTANTANEOUS DEVOLATILIZATION YIELD

With the solutions developed in the preceding two sections, we can now calculate the instantaneous rate of evolution of volatiles, the yield. First the yield will be expressed in terms of the position of the reactive interface. Then the asymptotic limits for large and small particles and high and low pressures will be presented, followed by more complete numerical solutions. The additional yield due to direct hydrogenation will be discussed in the next section.

The rate of production of volatiles is simply the flux of unreactive, or reacted, volatiles out of the particle; that is

$$N_v|_{r=a} = \frac{1}{3} ak_oC\ (1 - \pi x^c{}_{v^*}\lambda^3) \tag{63}$$

which can also be expressed as a fraction of the volatiles released as

$$\eta = \frac{4\pi a^2 N_v|_{r=a}}{\frac{4\pi a^3}{3} k_oC} = 1 - \pi x^c{}_{v^*}\lambda^3 \tag{64}$$

Now the two causes of reduced yield can be identified: high pressures which increase the deposition rate and large particles which have a significant core depleted of hydrogen. The asymptotic limits of the previous section further illustrate this point.

For sufficiently small particles, $\alpha < \alpha_{crit}$, and the yield will be unity, independent of pressure since $\lambda \equiv 0$. If, however, $\alpha > \alpha_{crit}$, the existence of a core introduces a strong pressure dependence. When $\pi << 1$, then $x^c{}_{v^*} \approx \nu$, and

$$\eta \simeq 1 - \nu\pi\lambda^3 \tag{65}$$

or for $\alpha^2(1 - \nu) >> 1$

$$\eta \approx 1 - \nu\pi\left[1 - \frac{9(1-\nu)}{\alpha^2} \ln\left(1 + \frac{1-\nu}{\nu} x^o{}_{H_2}\right)\right] \tag{66}$$

Even with the core occupying almost the entire particle, the yield is only slightly affected because of the slow deposition rate. The precise reduction in yield depends on the dimensionless particle size, the fraction of volatiles, and the hydrogen partial pressure. In the high pressure limit, $\pi >> 1$, $x^c{}_{v^*} \approx \nu/\pi$, and

$$\eta \approx 1 - \nu\lambda^3 \tag{67}$$

where λ and, therefore, the yield asymptote to constants independent of pressure but dependent on the other parameters. The numerical solutions presented below illustrate the smooth transition between these limits in the intermediate pressure range.

The full dependence of instantaneous yield on the pressure, particle size, and the fraction of reactive volatiles is illustrated in Figures 2 and 3. The yield is plotted as a function of π, the dimensionless pressure, with α^2, that is, the temperature and particle size, held constant. Only ν differs between the two graphs. In each case, the transition from mass transfer limited situations to kinetically limited ones occurs within a range of four orders of magnitude in π and less than three in α^2. The minimum hydropyrolysis yield at a given π

$$\eta = 1 - \pi x^c{}_{v^*} \tag{68}$$

obtains in the large particle limit $\alpha^2 \to \infty$ and coincides with the pyrolysis yield.

Figures 4 and 5 depict qualitatively the temperature dependence of the yield. Both reaction rates no doubt depend on temperature as does the diffusivity, but devolatilization might be expected to have a higher activation energy than the deposition rate and thus be more sensitive. Then, at constant pressure and particle size

$$\pi \propto e^{E_o/RT}$$

is inversely related to temperature, and

$$\alpha^2\pi = \frac{a^2 k_1 p_o}{p_o D_{eff}} \tag{69}$$

remains approximately constant. Thus the yield is high for $\pi >> 1$, corresponding to low temperatures and low devolatilization rates at which hydrogen easily permeates the particle to stabilize all reactive volatiles. As the temperature increases, a core forms, and deposition in the core reduces the yield as shown. With further increases in temperature, the rate of devolatilization at constant pressure increases faster than the deposition rate and so the yield recovers, even though the particle remains largely depleted of hydrogen. Thus, a minimum appears with its depth depending on $\alpha^2\pi$, a combination of pressure and particle size. As before, the pyrolysis yield provides a lower bound since there the core always occupies the entire particle.

The effect of particle size, mentioned repeatedly above, is isolated in Figure 6. With hydrogen the most dramatic effects appear at high pressures when the deposition reaction is relatively fast. The instantaneous pyrolysis yield, on the other hand, is predicted to be independent of particle size.

These trends in the instantaneous yield with pressure, particle size, and to some extent, temperature are in qualitative accord with the experimental results of Anthony and Howard at MIT and Graff et al. at CUNY. A quantitative comparison, however, requires two further steps which will be accomplished in the next section. These involve the direct hydrogenation yield and the transient nature of the devolatilization process which we recognized at the outset but temporarily set aside through the pseudo-steady state assumption.

RESULTS FOR OVERALL YIELD

To obtain the complete yield for devolatilization or hydropyrolysis, the instantaneous yield must be integrated over the time-temperature history of the particle and then added to the contribution from direct hydrogenation.

We can anticipate the qualitative effect of the time integration with the aid of Figure 5 depicting the yield vs.

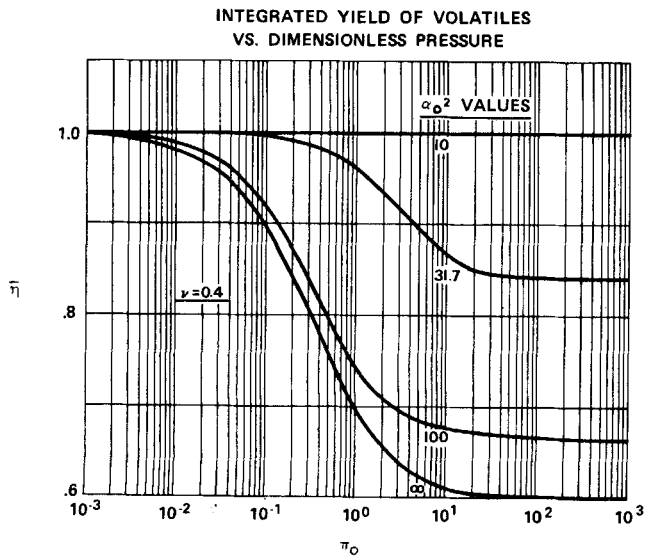

Fig. 7. Integrated yield of volatiles as function of dimensionless pressure π_0 with α_0^2 (temperature and particle size) constant (ν = 0.40): Single first-order decomposition.

π at constant pressure and particle size. Initially, the particle is cold and devolatilization slow; thus, $\pi >> 1$, and the few reactive volatiles which are generated escape. With heatup, the rate increases, π decreases at constant $\pi\alpha^2$, and a core forms with the deposition therein reducing the fractional yield. If the temperature becomes sufficiently high, the yield passes through the minimum and recovers, indicating that deposition in the core becomes slow relative to devolatilization. Eventually though, the reactive coal is depleted ($C \to 0$), again reducing the rate and driving the yield back through the minimum as $\pi \to \infty$. The ultimate yield thus depends on the time spent in the unfavorable reaction of η-π space during these two traverses.

This interpretation indicates two separate transients which affect the ultimate yield: the thermal relaxation of the particle and the kinetics of devolatilization. The initial sweep through the minimum is primarily governed by the heatup rate coupled with the temperature dependence of devolatilization. The second depends solely on the kinetics and the reaction time. Here we analyze only a portion of the problem, assuming instantaneous heatup and infinite reaction time.

Our motivation for initially ignoring the thermal transients derives from the experimental results of Anthony et al. (1976) with which our numerical predictions will

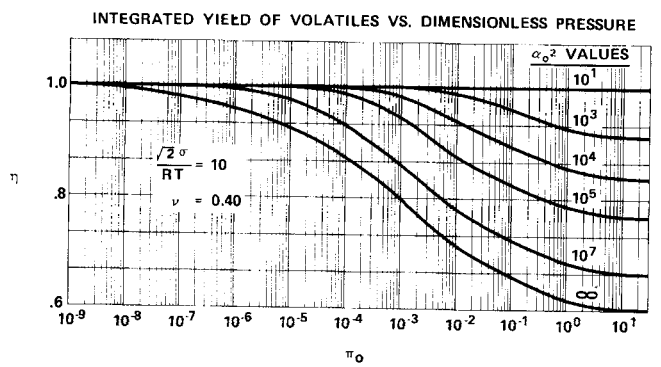

Fig. 8. Integrated yield of volatiles as function of dimensionless pressure π_0 with α_0^2 (temperature and particle size) constant (ν = 0.40): Spectrum of parallel first-order decompositions with Gaussian distribution of activation energies ($\sqrt{2}\sigma/RT$ = 10).

be compared. They usually employed long reaction times and observed little effect of heating rate above 600°C/s. The consequences of these assumptions will be discussed further in the last section.

Under isothermal conditions, the ultimate yield, normalized with the initial reactive coal C_o, is

$$\bar{\eta} = \int_0^\infty \eta k_o \frac{C}{C_o}\, dt \tag{70}$$

with the reactive coal remaining at time t determined by

$$\frac{dC}{dt} = -k_o C \tag{71}$$

with $C = C_o$ at $t = 0$. The fractional yield η must also be calculated at each time step from (52) and (64) because both π and α^2 depend on time through the amount of reactive coal C; that is

$$\pi = \pi_o \frac{C_o}{C}$$
$$\alpha^2 = \alpha^2{}_o \frac{C}{C_o} \tag{72}$$

where

$$\pi_0 = \frac{k_1 p_o}{k_o C_o RT}$$
$$\alpha_0{}^2 = \frac{a^2 k_o C_o RT}{p_o D_{eff}}$$

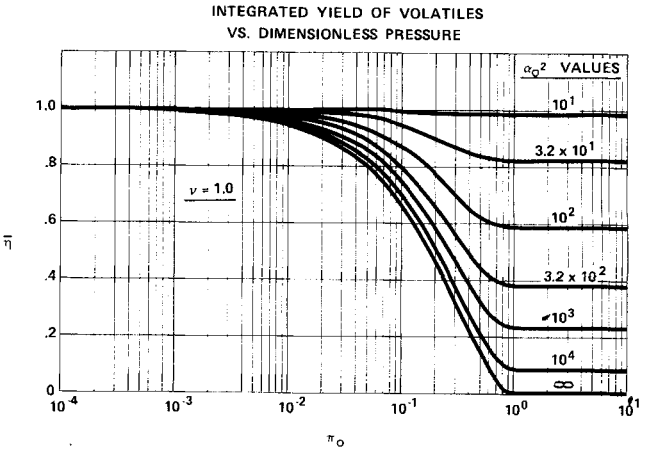

Fig. 9. Integrated yield of volatiles for single first-order decomposition with ν = 1.0, instantaneous heat up, and infinite reaction time: pressure effect.

Although written for a single devolatilization rate constant, these equations can easily be adapted to a set of parallel first-order reactions. The results discussed below were obtained by integrating (71) analytically, then numerically solving (52) for λ by Newton's method and integrating (70) using the trapezoidal rule. The asymptotic solutions presented earlier circumvented most numerical problems caused by the wide range of values encountered for both π and α^2. Step sizes and error limits were adjusted to achieve better than 1% accuracy in the yields.

Now we must consider the transient effects produced by the two kinetic models for devolatilization described earlier. Figure 7 depicts $\bar{\eta}$ vs. π_0 at constant α_0^2 for a single first-order decomposition with ν = 0.40. The curves closely resemble the instantaneous yields of Figures 2 and 3 except that the transition now stretches over a slightly wider range of π_0^2 and α_0^2. The analogous results for a set of parallel reactions with a Gaussian distribution of

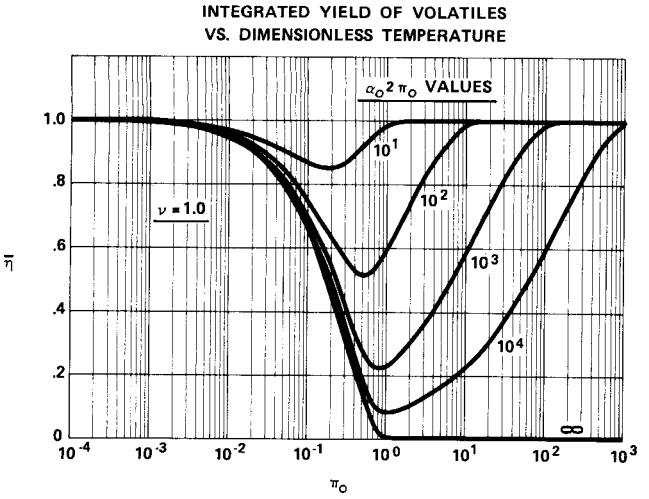

Fig. 10. Integrated yield of volatiles for single first-order decomposition with $\nu = 1.0$, instantaneous heat up, and infinite reaction time: temperature effect.

activation energies are graphed Figure 8. The dimensionless variance, $\sqrt{2}\sigma/RT = 10$, corresponds to Anthony and Howard's distribution for bituminous coal at 1 000°C, with the reactive volatiles assigned to the upper end of the spectrum. This causes the total devolatilization rate at a particular temperature to vary many orders of magnitude during the release of reactive volatiles; therefore, p must change by a comparable amount to complete the transition from kinetic to mass transfer control. The resulting weaker pressure dependence contrasts with their experiments in which the transition occurred within four decades in pressure. Thus, it appears that the single rate constant model predicts a more reasonable pressure dependence under isothermal reaction conditions.

With the single-reaction model, the parameters π_0 and α_0^2 fully determine the integrated yield. Figures 9 to 11 display the numerical results for $\bar{\eta}$ as a function of π_0 and α_0^2 or π_0 and $\pi_0\alpha_0^2$. Comparison with the corresponding Figures 2 through 6 for the instantaneous yield illustrates that the pressure, temperature, and particle size dependences remain qualitatively similar with some quantitative differences arising from the variation in devolatilization rate over the lifetime of the reaction. We now need only the direct hydrogenation yield to complete the theory.

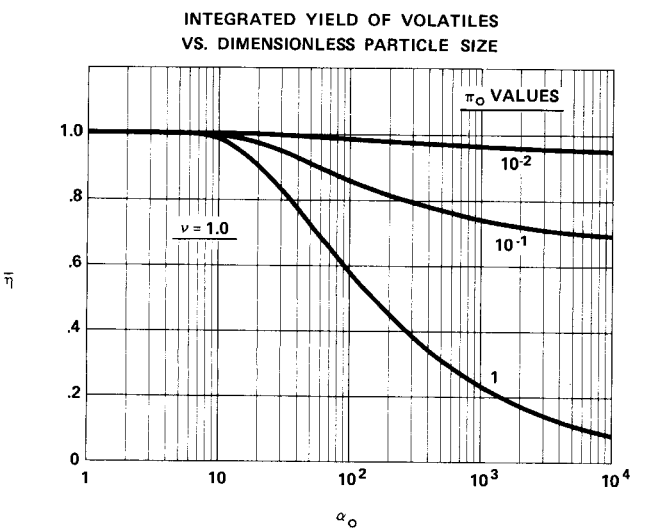

Fig. 11. Integrated yield of volatiles for single first-order decomposition with $\nu = 1.0$, instantaneous heat up, and infinite reaction time: particle size effect.

Our application of the Moseley and Paterson (1965) model for direct hydrogenation assumes the process to be much slower than devolatilization. The two reactions then proceed in series, with the latter essentially completed before the occurrence of appreciable direct hydrogenation. Diffusional limitations on hydrogen entering the particle can thus be ignored and (8) taken as the final yield at long residence times. When normalized by the molar density of potential volatiles in the original coal C_o, this becomes

$$\eta_d = \delta\pi_0 x^o_{H_2} \tag{73}$$

where

$$\delta = \frac{k_o k_3 C_o^*}{k_1 k_4}$$

The total yield

$$\bar{\eta} + \eta_d \tag{74}$$

with $\bar{\eta}$ from Figures 9 to 11 and η_d from (73) depends on five independent parameters (π_0, α_0^2, δ, $x^o_{H_2}$, and ν) determined by the process conditions and the particular coal properties. In the next section we illustrate how one can estimate these from experimental data and then compare the theoretical predictions to observed trends in yield.

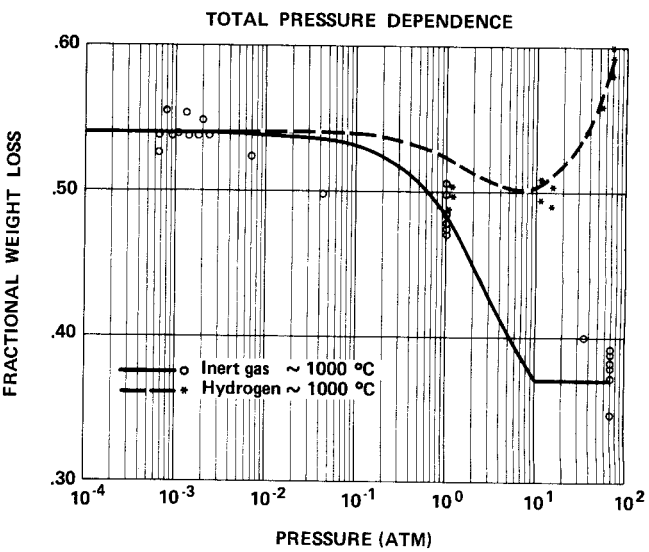

Fig. 12. Comparison of theoretical predictions (solid and dashed lines) with weight loss data of Anthony et al. (1976): pressure dependence.

COMPARISON WITH EXPERIMENTAL DATA

Evaluation of the theory requires a complete set of experimental data in which process conditions have been varied systematically over a wide range. In this initial study, we focus on the weight loss data of Anthony et al. (1976) at MIT. Extensions to other experimental systems and more detailed predictions of product distributions remain for future work.

First the parameters in the model must be determined in a straightforward manner. Process variables such as pressure, temperature, particle size, and hydrogen partial pressure cause no difficulty because they are measured directly. The preexponential factor and activation energy for the devolatilization step were determined at MIT from kinetic data as

$$A_0 = 1\,800\ \text{s}^{-1}$$
$$E_0 = 5.57 \times 10^7\ \text{J/kg·mole} \tag{75}$$

The relevant fraction of reactive volatiles, however, is not quite so clear.

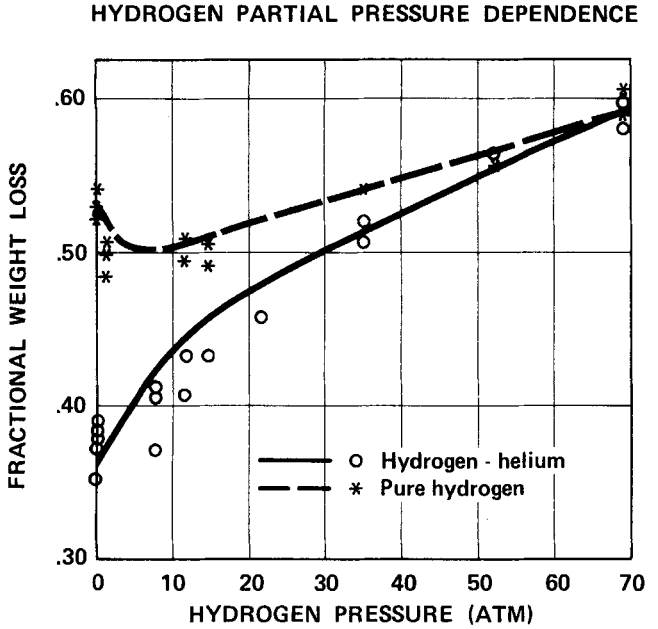

Fig. 13. Comparison of theoretical predictions (solid and dashed lines) with weight loss data of Anthony et al. (1976): hydrogen partial pressure dependence.

The MIT pyrolysis data in Figure 12 indicate that reactive volatiles form about 32% of the potential volatiles yield, but weight loss vs. time and temperature curves strongly suggest that these species are liberated at longer times and higher temperatures than the unreactive volatiles. We, therefore, treat these as two separate first-order reactions with quite different rates so that unreactive volatiles essentially disappear before the release of reactive volatiles begins. Thus $\nu = 1.0$, rather than $\sim .32$, during the latter process. We still apply the above kinetic parameters, but this only affects the temperature dependence of our predictions.

There still remain three combinations of unknown parameters in the dimensionless groups π_0, δ, and α_0^2, that is

$$\frac{k_1}{C_o} \qquad \frac{k_3 C_o^*}{k_4 C_o} \qquad \frac{p_o D_{eff}}{C_o} \tag{76}$$

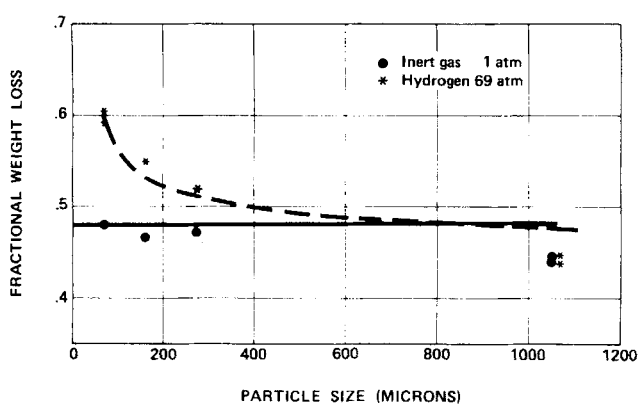

Fig. 14. Comparison of theoretical predictions (solid and dashed lines) with weight loss data of Anthony et al. (1976): particle size dependence.

These can be estimated from the pressure dependence of the pyrolysis yield, the hydropyrolysis yield for large particles, and the high pressure asymptote of the hydropyrolysis yield for small particles.

First, for pyrolysis (Figure 12) an increase in pressure from 10^{-3} to 1.0 atm reduces the fraction of reactive volatiles escaping from 1.00 to 0.66. Comparison with Figure 9 discloses that

$$\frac{k_1}{k_o C_o RT} = 1.45 \times 10^{-3}\ \text{atm}^{-1}$$

or

$$\frac{k_1}{C_o} = 9.5 \times 10^{1}\ \frac{\text{m}^3}{\text{kg·mole·s}} \tag{77}$$

Next we note that in Figure 13 the hydropyrolysis yield for large particles at 69 atm lies about 8 to 10 wt % carbon above the pyrolysis yield at the same conditions. Since no reactive volatiles escape in either case, this must reflect direct hydrogenation, indicating from (73) that

$$\frac{k_3 C_o^*}{k_4 C_o RT} = 10^{-1}\ \text{atm}^{-1}$$

or

$$\frac{k_3 C_o^*}{k_4 C_o} = 1.45 \times 10^{-1}\ \frac{\text{m}^3}{\text{kg·mole}} \tag{78}$$

Finally we turn to the hydropyrolysis yield for small particles in Figure 12. Subtraction of the direct hydrogenation contribution must leave a constant high pressure

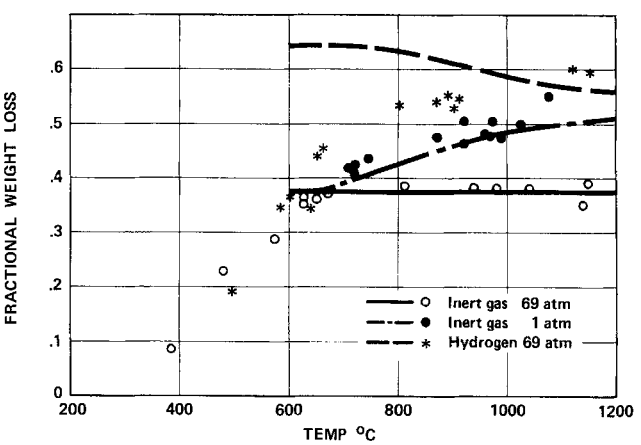

Fig. 15. Comparison of theoretical predictions (solid and dashed lines) with weight loss data of Anthony et al. (1976): temperature dependence.

asymptote as predicted by Figure 9. The value obtained from the data, 50 wt % carbon, determines

$$\alpha_0^2 = 56.5$$

or

$$\frac{p_o D_{eff}}{C_o} = 8.6 \times 10^{-9}\ \frac{\text{atm-m}^5}{\text{kg·mole·s}} \tag{79}$$

Since the detailed predictions are fairly sensitive to the magnitudes of these three adjustable parameters, it is reassuring to note the agreement with independent estimates for similar systems. First, by coupling a reasonable density of 1.5×10^3 kg/m^3 for the original coal with a mean molecular weight of ~ 30 kg/kg mole (corresponding to ethane) for the volatile products, one can obtain

$$C_o \simeq 5 \times 10^{-1}\ \frac{\text{kg mole}}{\text{m}^3}$$

and

$$p_o D_{eff} \simeq 4.3 \times 10^{-7}\ \frac{\text{atm-m}^2}{\text{s}} \tag{80}$$

Comparison with the values presented earlier for the pressure-diffusivity product indicates a geometrical factor for the pore structure of the coal particle of

$$K_1 \sim 10^{-2}$$

a somewhat low but not unreasonable value. For the direct hydrogenation of char at 1 000°C and 500 atm, Moseley and Paterson (1965) found 70% carbon conversion which translates into

$$\frac{k_3}{k_4} = 1.5 \times 10^{-1} \frac{\text{m}^3}{\text{kg mole}} \tag{81}$$

If $C_o^* \approx C_o$, the agreement with (78) is almost exact.

The solid curves in Figures 12 to 15 represent our theoretical predictions based on the preceding values for the model parameters. Figures 12 and 13 display the pressure dependence. The upper curve in the latter graph pertains to hydrogen at the pressure shown and the lower to hydrogen-helium mixtures at 69 atm total pressure. The theory somewhat overestimates the yield at ambient and moderately subambient pressures, but the overall agreement is as good or better than with Anthony and Howard's theory.

A significant achievement is the successful explanation of the particle size effect in Figure 14. Indeed, extrapolation to zero radius indicates a potential carbon conversion of 64% at 69 atm and 1 000°C, provided the direct hydrogenation yield remains independent of particle size. The discrepancy between the theory and the data with large particles cannot be removed by adjusting the parameters but could be the result of slower heating due to longer thermal response times.

The temperature dependence of the yield illustrated in Figure 15 prompted Anthony and Howard to use the parallel reaction model with the higher activation energies ascribed to those decompositions producing reactive volatiles. Then the increased yield with higher temperatures but fixed residence times can be rationalized as a kinetic effect. Our theory, based on instantaneous heatup and infinite reaction times with only a single first-order decomposition, predicts the correct pyrolysis trends as mass transfer effects but fails for hydropyrolysis. The reason is clear from the curves in Figure 10. At 69 atm and 1 000°C, $\pi_0 = 6.9$, and yields from pyrolysis and hydropyrolysis lie near a minimum. With decreasing temperature π_0 increases, raising the hydropyrolysis yield while that for pyrolysis remains constant. Consistent accommodation of both the temperature and pressure trends will require a more sophisticated treatment of both the time-temperature history and the devolatilization kinetics.

The present theory provides a fundamental description of mass transfer processes within an individual coal particle which were implicit in the earlier model of Anthony et al. (1976). In essence, their transfer coefficients (empirical constants in their analysis) are related explicitly to the devolatilization rate and the physical properties of the coal. As a result, the particle size dependence is predicted for the first time. Temperature effects for hydropyrolysis are handled less satisfactorily with the idealized time-temperature history and rate expression. Clearly, further work should incorporate finite heating rates and reaction times with more realistic devolatilization kinetics, for example, a statistical distribution of activation energies or production rates for individual species from Suuberg (1977).

ACKNOWLEDGMENT

The authors would like to thank the Cities Service Research and Development Company for its financial and technical support in the development of the model.

NOTATION

a = radius of coal particle
A_o = preexponential factor for devolatilization reaction
B_o = Darcy permeability
C, C_o = instantaneous and total molar densities of reactive coal in particle
C^*, C_o^* = instantaneous and total molar densities of activated coal in particle
c_1, c_2 = integration constants
D_{ij} = binary gas phase diffusion coefficient
D^e_{ij}, D_{eff} = effective diffusion coefficients within porous particle
E_o, E = activation energy for devolatilization reaction
$f(E)$ = distribution function for activation energies of multiple parallel reactions
$g(x)$ = dimensionless function defined by Equation (48)
h = particle-to-gas heat transfer coefficient
k_o = devolatilization rate constant
k_1 = deposition rate constant
k_2 = stabilization rate constant
k_3 = direct hydrogenation rate constant
k_4 = polymerization rate constant
K_1 = geometrical factor for pore structure ($= \phi/\tau$)
M_j = molecular weight of j^{th} species
N_j = radial molar flux of j^{th} species with respect to fixed coordinates
p = total pressure
p_o = bulk gas pressure
Pr = Prandtl number for gas
r = radial position within particle
R = gas constant
R_j = rate of production of j^{th} species by chemical reaction
t = time
T = temperature
x_j, x_j^o = local and external mole fractions of j^{th} species

Greek Letters

α = thermal diffusivity
λ = dimensionless position of reaction interface
$\eta, \overline{\eta}$ = instantaneous and total fractions of volatiles escaping from particle
η_d = direct hydrogenation yield normalized by volatiles yield
ϕ = porosity of particle
τ = tortuosity of pores within particle
μ = viscosity of gas
ρc_p = volumetric thermal capacity
ν = fraction of volatiles which are reactive

Dimensionless Groups

$$\pi = \frac{k_1 p_o}{k_o C\,RT} = \frac{C_o}{C}\,\pi_o$$

$$\alpha^2 = \frac{a^2 k_o C\,RT}{p_o D_{\text{eff}}} = \frac{C}{C_o}\,\alpha_o^2$$

$$\epsilon = \frac{a^2 \mu k_o C\,RT}{p_o^2 B_o}$$

$$\beta = \frac{k_3 C_o^* p_o}{k_o C\,RT}$$

$$\delta = \frac{k_o k_3 C_o^*}{k_1 k_4}$$

$$\overline{r} = r/a$$

$$y = \alpha^2(\lambda - \overline{r}\,)$$

$$\overline{p} = \frac{p - p_o}{\epsilon p_o}$$

$$\overline{N_i} = \frac{Ni}{ak_oC}$$

Subscripts

s = solid coal
g = gas
H_2 = hydrogen
I = inert gas
v = stable volatiles
v^* = reactive volatiles

Superscripts

c = value in core
λ = value at reaction interface

LITERATURE CITED

Anthony, D. B., "Rapid Devolatilization and Hydrogasification of Pulverized Coal," Sc.D. thesis, Dept. Chemical Engineering, Mass. Inst. Technol., Cambridge (1974).

———, and J. B. Howard, "Coal Devolatilization and Hydrogasification," *AIChE J.*, **22**, 625 (1976).

———, H. C. Hottel, and H. P. Meissner, "Rapid Devolatilization and Hydrogasification of Bituminous Coal," *Fuel*, **55**, 121 (1976).

Aris, R., *The Mathematical Theory of Diffusion and Reaction in Permeable Catalysts*, Clarendon Press, Oxford, England (1975).

Badzioch, S., D. R. Gregory, and M. A. Field, "Investigation of the Temperature Variation of the Thermal Conductivity and Thermal Diffusivity of Coal," *Fuel*, **43**, 267 (1964).

Benson, S. W., *The Foundations of Chemical Kinetics*, McGraw-Hill, New York (1960).

Dutta, S., C. Y. Wen, and R. J. Belt, "Reactivity of Coal and Char in CO_2 Atmosphere," *Am. Chem. Soc., Div. of Fuel Chem. Preprints*, **20**, No. 3, 103 (1975).

Graff, R. A., S. Dobner, and A. M. Squires, "Flash Hydrogenation of Coal: 1. Experimental Methods and Preliminary Results; 2. Yield Structure for Illinois No. 6 Coal at 100 atm," *Fuel*, **55**, 109, 113 (1976).

Greene, M. I., "Engineering Development of the Cities Service, Short Residence Time (CS-SRT) Process," *Am. Chem. Soc., Div. of Fuel Chem. Preprints*, **22**, No. 7, 133 (1977).

Hirschfelder, J. O., C. F. Curtiss, and R. B. Bird, *Molecular Theory of Gases and Liquids*, Wiley, New York (1954).

Hite, R. H., and R. Jackson, "Pressure Gradients in Porous Catalyst Pellets in the Intermediate Diffusion Regime," *Chem. Eng. Sci.*, **32**, 703 (1977).

Hutchings, J., and J. J. Carberry, "The Influence of Surface Coverage on Catalyst Effectiveness and Selectivity. The Isothermal and Nonisothermal Cases," *AIChE J.*, **12**, 20 (1966).

Johnson, J. L., "Kinetics of Bituminous Coal Char Gasification with Gases Containing Steam and Hydrogen," in *Coal Gasification*, p. 145, Advances in Chemistry Series, No. 131, Am. Chem. Soc., Washington, D.C. (1974).

Loison, R., A. Peytary, A. F. Bower, and R. Grillot, "The Plastic Properties of Coal," in *Chemistry of Coal Utilization*, Supplementary Vol., H. H. Lowry, ed., p. 150, New York (1963).

Mason, E. A., A. P. Malinauskas, and R. B. Evans, III, "Flow and Diffusion of Gases in Porous Media," *J. Chem. Phys.*, **46**, 3199 (1967).

Mazamdar, B. K., and N. N. Chatterjee, "Mechanism of Coal Pyrolysis in Relation to Industrial Practice," *Fuel*, **52**, 11 (1973).

Moseley, F., and D. Paterson, "The Rapid High-Temperature Hydrogenation of Coal Chars, Part 2: Hydrogen Pressures up to 100 Atmospheres," *J. Inst. Fuel*, **38**, 378 (1965).

Nusselt, W., "Die Verbrennung und die Vergassung der Kohle auf dem Rost," *Ver. Deut. Ing.*, **60**, 102 (1916).

Reid, R. C., and T. K. Sherwood, *The Properties of Gases and Liquids*, McGraw-Hill, New York (1958).

Scheidegger, A. E., *The Physics of Flow through Porous Media*, Univ. Toronto, Canada (1960).

Steinberg, M., and P. Fallon, "Coal Liquefaction by Rapid Gas Phase Hydrogenation," *Am. Chem. Soc., Div. of Petroleum Chem. Preprints*, **20**, No. 2, 542 (1975).

Suuberg, E. M., W. A. Peters, and J. B. Howard, "Product Composition and Kinetics in Lignite Pyrolysis," *Am. Chem. Soc., Div. of Fuel Chem. Preprints*, **22**, No. 1, 112 (1977).

Van Krevelen, D. W. F., *Coal*, Elsevier, Amsterdam (1961).

Vand, V., "A Theory of the Irreversible Electrical Resistance Changes of Metallic Films Evaporated in Vacuum," *Proc. Phys. Soc. (London)*, **A55**, 222 (1943).

Zahradnik, R. L., and R. A. Glenn, "Direct Methanation of Coal," *Fuel*, **50**, 77 (1971).

Manuscript received December 5, 1977; revision received August 11, and accepted August 25, 1978.

Continuous Phase Mass Transfer During Formation of Drops from Jets

This study enables the extension of a recent design procedure for perforated plate extraction columns to include operation under jetting conditions. Correlations of experimental data are given for jet length, jet contraction, drop size, and mass transfer rates in continuous phase controlled liquid-liquid systems. Systems exhibiting very low mass transfer rates were used, and this gave significantly different results from those obtained earlier with moderate rates of mass transfer.

A. H. P. SKELLAND

and

Y-F. HUANG

Chemical Engineering Department
The University of Kentucky
Lexington, Kentucky 40506

SCOPE

A method for the design of perforated plate extraction columns was published recently by Skelland and Conger (1973). The procedure is in terms of rate equations and relevant hydrodynamics and, after machine computation using Fortran IV language, yields the number of real plates required for a given separation, the column diameter, the number of holes per plate, and the cross-sectional area of the downcomers. In view of Mayfield and Church's

0001-1541-79-1689-0080-$00.95.